Solution conformation of an essential region of the p53 transactivation domain

Maria Victoria E Botuyan[1], Jamil Momand[2] and Yuan Chen[1]

Background: The peptide segment surrounding residues Leu22 and Trp23 of the p53 transactivation domain plays a critical role in the transactivation activity of p53. This region binds basal transcriptional components such as the TATA-box binding protein associated factors $TAF_{II}40$ and $TAF_{II}60$ as well as the mdm-2 and adenovirus type 5 E1B 55 kDa oncoproteins.

Results: The structure of residues 14–28 of p53 was studied by nuclear magnetic resonance spectroscopy and found to prefer a two-β-turn structure stabilized by a hydrophobic cluster consisting of residues known to be important for transactivation and binding to p53-binding proteins. A peptide segment in which Leu22 and Trp23 were replaced by Gln and Ser displays a random structure.

Conclusions: This structural propensity observed in the wild-type p53 peptide is important for understanding the mechanism of transcriptional activation, because very few structural data are available on transactivation domains to date. These results should aid in the design of therapeutics that could competitively inhibit binding of p53 to the oncogene product mdm-2.

Addresses: [1]Division of Immunology, Beckman Research Institute of the City of Hope, Duarte, CA 91010, USA. [2]Department of Cell & Tumor Biology, City of Hope National Medical Center, Duarte, CA 91010, USA.

Correspondence: Yuan Chen
E-mail: yuan@bloch.coh.org

Key words: mdm-2, p53, structural propensity, TAF

Received: **03 June 1997**
Revisions requested: **26 June 1997**
Revisions received: **17 July 1997**
Accepted: **22 July 1997**

Published: **20 October 1997**
http://biomednet.com/elecref/1359027800200331

Folding & Design 20 October 1997, **2**:331–342

Introduction

The p53 tumor suppressor protein is a checkpoint protein that responds to cellular stress [1,2]. p53 directly binds and upregulates genes that arrest the cell cycle or activate an apoptotic pathway [3,4]. The N-terminal 40 amino acid residues of p53 are capable of conferring transactivation function when fused onto a heterologous DNA-binding domain [5–7]. The p53 transactivation domain binds TFIID, the multimeric protein complex responsible for directing RNA polymerase II-mediated transcription. Polypeptides within TFIID such as the TATA-box binding protein (TBP) and two TBP-associated factors (TAFs), $TAF_{II}40$ and $TAF_{II}60$, have been shown to specifically bind p53 [8–11]. This p53 domain also binds proteins that inhibit its transactivation. Mdm-2, a cellular oncoprotein upregulated in a variety of cancers [12,13], and the adenovirus oncoprotein E1B 55 kDa (E1B 55K) have been shown to block p53-mediated transactivation [14,15] through binding this p53 domain [16–19].

Extensive mutagenesis studies have identified residues 14–28 of p53 as a critical region for transactivation and binding of these proteins [7,9–11,18]. A peptide corresponding to residues 16–25 of p53 was shown to independently bind mdm-2 [19]. It is not unexpected that this short peptide can duplicate this function of intact p53, as circular dichroism (CD) and proteolytic digestion studies revealed that the p53 transactivation domain does not have a compactly folded tertiary structure [7,20]. In this situation, the local structure and function of a peptide segment is not affected by distal residues. Therefore, structural and functional properties of a peptide corresponding to this region of p53 (residues 14–28) should be similar to those in an intact p53 molecule. This region of p53 also contains an antibody-binding site [19]. A number of immunogenic and antigenic peptides have been shown to have conformational preferences for structured forms [21].

Although the conformational preferences of short linear peptide fragments may not always reflect their conformations when bound to receptor proteins or in the original proteins, many studies have shown that the structural propensity, detected by CD or NMR spectroscopy, often reflects the conformations of a peptide in the original protein or when bound to a physiological receptor [22,23]. If a peptide prefers a conformation similar to its receptor-bound state, it will more readily bind to the receptor compared to a peptide that lacks structural propensity. If a peptide lacks structural propensity, it must search for a large number of possible conformations to find the receptor-bound one, a process that is both time and entropy consuming. Similarly, if a peptide has the propensity to form a conformation similar to that in the native protein, it can serve as a nucleation site in protein folding [24,25]. The structure of a peptide corresponding to residues 15–29 of p53 bound to mdm-2 has been studied by X-ray crystallography [26]. The conformation of a peptide corresponding to residues 17–24 of p53 when bound to mdm-2 has also been investigated by transfer NOE studies [27]. The conformations of p53 bound to $TAF_{II}40$, $TAF_{II}60$

and oncoprotein E1B 55K have not been reported, however. The structural preference of the critical region of p53, residues 14–28, may reflect the conformations of p53 in complexes with these proteins. Knowledge of the structural propensity of this region of p53 in the free form would improve our understanding, on the molecular level, of the mechanisms by which p53 interacts with TFIID and oncoproteins mdm-2 and E1B 55K.

Many peptides have been shown to have structurally preferred conformations, although most short linear peptides are completely random in solution. The structural propensity of peptides may originate from the intrinsic preferences of amino acid residues for certain dihedral angles [28]. The propensity may also result from amino acid sidechain interactions that lead to a deviation of the backbone dihedral angles from random-coil values [29]. The principles for predicting conformational propensities in peptides on the basis of their amino acid sequences are still under intensive study.

In order to evaluate the conformational propensities of the Leu14–Glu28 region of p53, we conducted NMR studies on a synthetic peptide (LSQETFSDLWKLLPE) of human p53. We found that this region has a significant propensity to cooperatively form two successive β turns stabilized by a hydrophobic cluster. Previous studies showed that the double substitution Leu22→Gln Trp23→Ser is the only mutation, thus far, that curtails p53 interactions with the TAFs, mdm-2 and E1B 55K, as well as p53-mediated transactivation. We also examined the conformational properties of an identical length synthetic peptide where Leu22 and Trp23 were replaced by Gln and Ser (LSQETFSDQSKLLPE). We found that the mutant peptide is completely random, due to the disruption of the hydrophobic cluster.

Results

Evaluation of sample conditions

Short linear peptides may aggregate at high concentrations. In order to determine that the peptides being studied are in the monomeric form under the conditions of our NMR studies, the NMR measurements were conducted at peptide concentrations from 0.2 mM to 10 mM. No concentration-dependent changes in proton chemical shifts, resonance linewidths or NOEs have been observed. In addition, the linewidths of proton resonances of both the wild-type and mutant p53 peptides are appropriate for monomeric forms of both peptides.

In order to further confirm that the peptides being studied are in the monomeric forms, the diffusion coefficients of the peptides at 10 mM concentration were measured using the pulsed-field gradient method [30]. The gradient field strengths were calibrated carefully using a 2 mM lysozyme sample (D_s = 1.08×10^{-6} cm^2/s at 25°C). Ten gradient strengths were used as described in the Materials and methods section and the resulting spectra are shown in Figure 1a. The plots of ln(echo amplitudes), ln(A), versus the square of the gradient field strengths, g^2, are shown in Figure 1b for both the wild-type and mutant p53 peptides measured at 2°C and for lysozyme measured at 25°C. The diffusion coefficients of the wild-type and mutant p53 peptides are 1.23×10^{-6} and 1.15×10^{-6} cm^2/s, respectively, at 2°C. The hydrodynamic radii estimated from the diffusion coefficients are similar to those of monomeric peptides of similar sizes measured by light scattering at 20°C [31].

Resonance assignments of the wild-type and mutant p53 peptides were performed using the established approaches

Figure 1

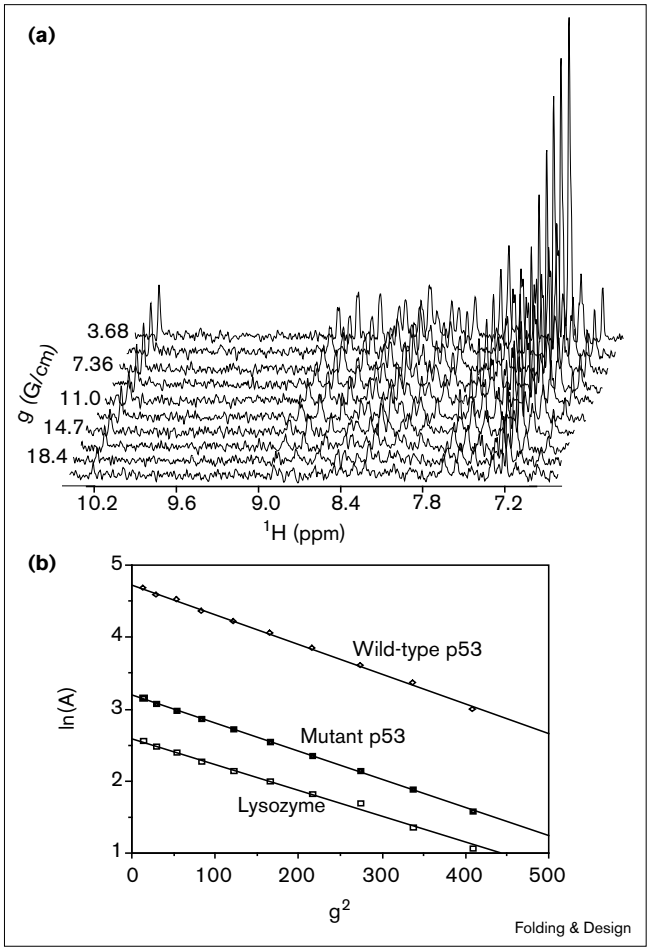

(a) Stack plots of the pulsed-field NMR spectra at 10 gradient (g) strengths: 3.68, 5.52, 7.36, 9.92, 11.0, 12.9, 14.7, 16.6, 18.4, and 20.2 Guass/cm. The sample contained 10 mM wild-type p53 peptide dissolved in D_2O with 10 mM sodium phosphate buffer, pH 6.0. **(b)** Plots of ln(echo amplitudes), ln(A), versus the square of the gradient field strengths, g^2, of the wild-type and mutant p53 peptides and lysozyme. The data for lysozyme were acquired at 25°C, and the data for the peptides were acquired at 2°C.

Figure 2

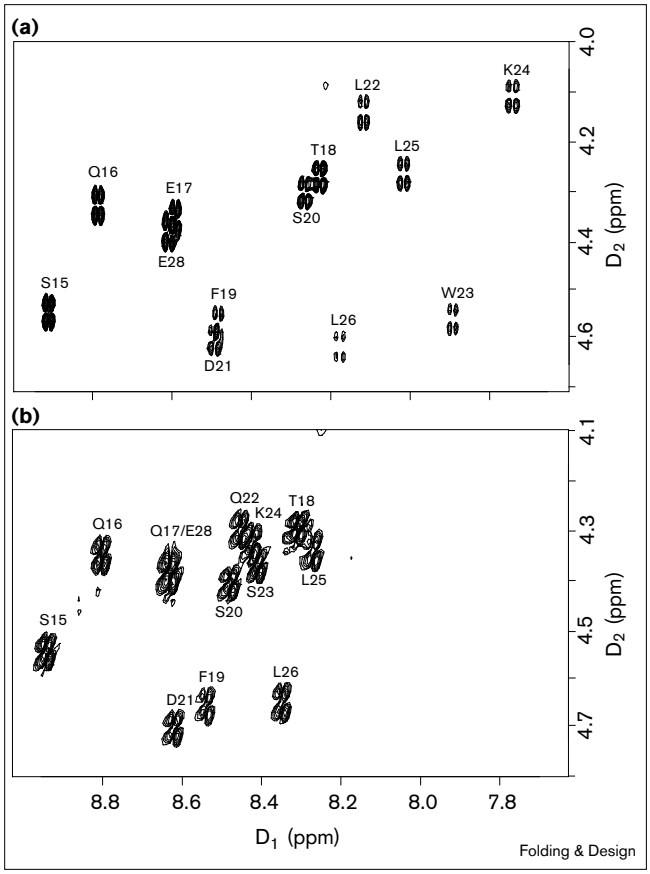

Fingerprint regions of the DQF-COSY spectra of **(a)** wild-type and **(b)** mutant p53 peptides. The spectra were taken at 2°C with samples in 90%H_2O/10%D_2O and 10 mM sodium phosphate buffer, pH 6.0.

Figure 3

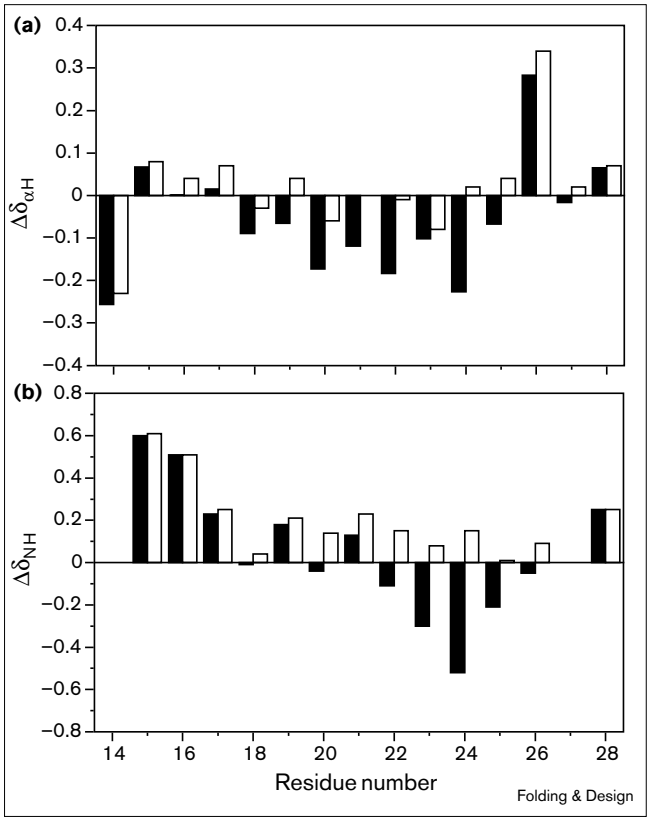

Plots of the difference in NMR chemical shift (observed – random coil) for **(a)** αH and **(b)** NH versus residue number. The filled bars and open bars correspond to the wild-type and mutant peptides, respectively.

[32]. The proton chemical shifts are referenced to 2,2-dimethyl-2-silapentane-5-sulfonic acid (DSS). Fingerprint regions of the DQF-COSY spectra of the wild-type and mutant p53 peptides are shown in Figure 2. Residues 18–25 display the largest differences (≥ 0.06 ppm) in the αH chemical shifts between the wild-type and the mutant p53 peptides. The amide proton chemical shifts of residues 20–26 differ by more than 0.1 ppm between the two peptides. Residues at both termini have similar backbone proton chemical shifts between the two peptides, however. Only one strong crosspeak for each residue has been found. Several smaller crosspeaks with intensities less than 5% of the major peaks have also been observed. These peaks may result from impurities or minor conformations.

The differences between the peptide backbone proton chemical shifts and their random-coil values provide an estimation of their secondary structures [33]. Deviations of αH chemical shifts from the random-coil values for the wild-type and mutant p53 peptides are shown in Figure 3a. Both αH and NH random-coil chemical shifts are taken from Wishart and Sykes [33]. The αH protons from residues 18–25 of the wild-type p53 peptide are uniformly upfield-shifted, whereas the αH chemical shifts of the mutant peptide are randomly distributed and generally close to the random-coil values. The αH resonance of residue 26 is shifted downfield by 0.29 and 0.34 ppm in the wild-type and mutant p53 peptides, respectively, presumably due to the presence of Pro27 [34]. It has been found that the mean deviation of αH chemical shifts from the random-coil values for the 20 naturally occurring amino acids is –0.39 ppm when placed in a helical configuration. In the β-strand configuration, this mean deviation is 0.37 ppm. The observed uniformly upfield-shifted αH chemical shifts of the wild-type peptide may indicate some preference for the α-helical configuration. No deviations are larger than 0.3 ppm, however, indicating that the wild-type peptide has no strong tendency for α-helix formation. The deviation of NH chemical shifts from random-coil values gives information on hydrogen bonding. Partial desolvation of an NH proton or formation of an intramolecular hydrogen bond, which has a lower strength than hydrogen bonds with solvent water molecules, results in upfield-shifted NH

Figure 4

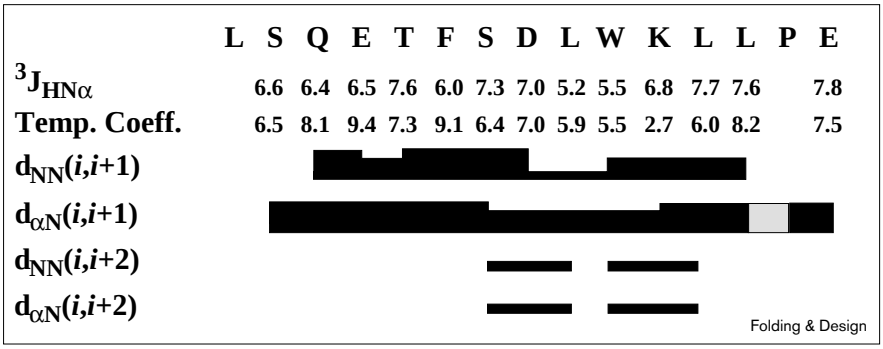

Schematic diagram showing the sequential and medium-range NOEs between backbone protons. Also shown are coupling constants, $^3J_{HN\alpha}$, in Hz (±1.2 Hz) and temperature coefficients, $\Delta\delta$, in ppb/K (±0.3 ppb/K). The light-gray box indicates the connectivity observed to δH of the Pro residue in place of the amide proton.

resonances relative to the random-coil values. The deviation of amide proton chemical shifts from random-coil values of both the wild-type and mutant p53 peptides are shown in Figure 3b. Residues *22*–*25* of the wild-type p53 peptide are significantly upfield shifted, indicating partial desolvation or formation of intramolecular hydrogen bonds by these residues.

NOEs, coupling constants and temperature coefficients

A series of NOESY spectra with mixing times ranging from 50 to 500 ms were recorded for the wild-type peptide in order to find the appropriate mixing time for structural analysis. It was found that the 300 ms mixing time is in the linear region of the NOE build-up curve. Therefore, NOEs were analyzed from the 300 ms mixing time NOESY spectrum. Characteristic sequential and medium-range NOEs give information about secondary structures. In β strands, $d_{\alpha N}(i,i+1)$ NOEs are observed, but $d_{NN}(i,i+1)$ NOEs are generally not observed. In helical structures, both NOEs can be observed. Additionally, $d_{\alpha\beta}(i,i+3)$ and $d_{\alpha N}(i,i+3)$ NOEs are characteristic for helical conformations. A schematic diagram showing the sequential and medium-range NOEs between backbone protons is presented in Figure 4. The $d_{\alpha N}$ and d_{NN} regions of the NOESY spectrum of the wild-type p53 peptide are shown in Figure 5. Sequential $d_{\alpha N}$ and d_{NN} connectivities have been observed for the wild-type and the mutant p53 peptides. The presence of both $d_{NN}(i,i+1)$ and $d_{\alpha N}(i,i+1)$ NOE connectivities indicates that the conformational ensembles of the peptides in solution have no tendency for forming extended β strands. Although both $d_{NN}(i,i+1)$ and $d_{\alpha N}(i,i+1)$ NOEs can be observed in helical structures, characteristic $d_{\alpha\beta}(i,i+3)$ or $d_{\alpha N}(i,i+3)$ NOEs were not detected. Detection of some of these NOEs could be hampered by signal overlapping. But the signals that are not in the overlapped region, for example the $d_{\alpha N}(i,i+3)$ NOE between Ser20 and Trp23, were not observed. Thus, it appears that there is no strong tendency for the peptides to form a helical conformation. The peptide bond proceeding Pro27 appears to be mainly in the *trans* conformation, because the $d_{\alpha\delta}$ NOE was observed but no detectable $d_{\alpha\alpha}$ NOE was observed.

Evidence for turn structures in the wild-type p53 peptide has been found. Two $d_{\alpha N}(i,i+2)$ NOEs have been observed between Ser20 and Leu22 and between Trp23 and Leu25 in the wild-type peptide. In addition, the $d_{NN}(i,i+2)$ NOEs have also been observed for the two pairs of residues (Figure 5). In type I and type II β turns, $d_{\alpha N}(i,i+2)$ distances between residues 2 and 4 are 3.2 Å and 3.6 Å, respectively. The $d_{NN}(i,i+2)$ distances between residues 2 and 4 are 3.8 Å and 4.3 Å, respectively. Both turns have strong $d_{NN}(3,4)$ NOEs. The two types of turns may be distinguished by comparing the intensities of $d_{NN}(2,3)$ and $d_{\alpha N}(2,3)$ NOEs. The $d_{NN}(2,3)$ is stronger than the $d_{\alpha N}(2,3)$ NOE in type I turns, and the reverse for type II turns. The $d_{\alpha N}$ NOE intensities are stronger than that of the $d_{NN}(2,3)$ between residues 20 and 21 and between residues 23 and 24. These data suggest type II turns, but the coupling constants, discussed below, are not consistent with type II turns.

Although the mutant p53 peptide has only two amino acid substitutions, medium-range or long-range NOEs were not observed for either the backbone protons or the sidechain protons. This suggests that the mutant peptide does not have detectable structural propensity. This is consistent with the backbone proton chemical shifts being similar to random-coil values.

Although *i* to *i+2* NOEs between backbone protons may be observed even when the peptide displays random-coil structures due to transient encounter of these protons [35], coupling constant measurements of the wild-type p53 peptide provide strong support that the wild-type p53 peptide deviates significantly from the random-coil structure. The $J_{HN\alpha}$ coupling constants were measured for 13 residues of the wild-type p53 peptide. Phe19, Leu22 and Trp23 have coupling constants between 5 Hz and 6 Hz (Figure 4). These coupling constants are significantly below the intrinsic coupling constants for these residues in a random-coil structure [36,37], indicating that appreciable conformational preference exists around residues 19, 22 and 23. These residues are part of both turns suggested by NOE data. Coupling constants for other residues are all

Figure 5

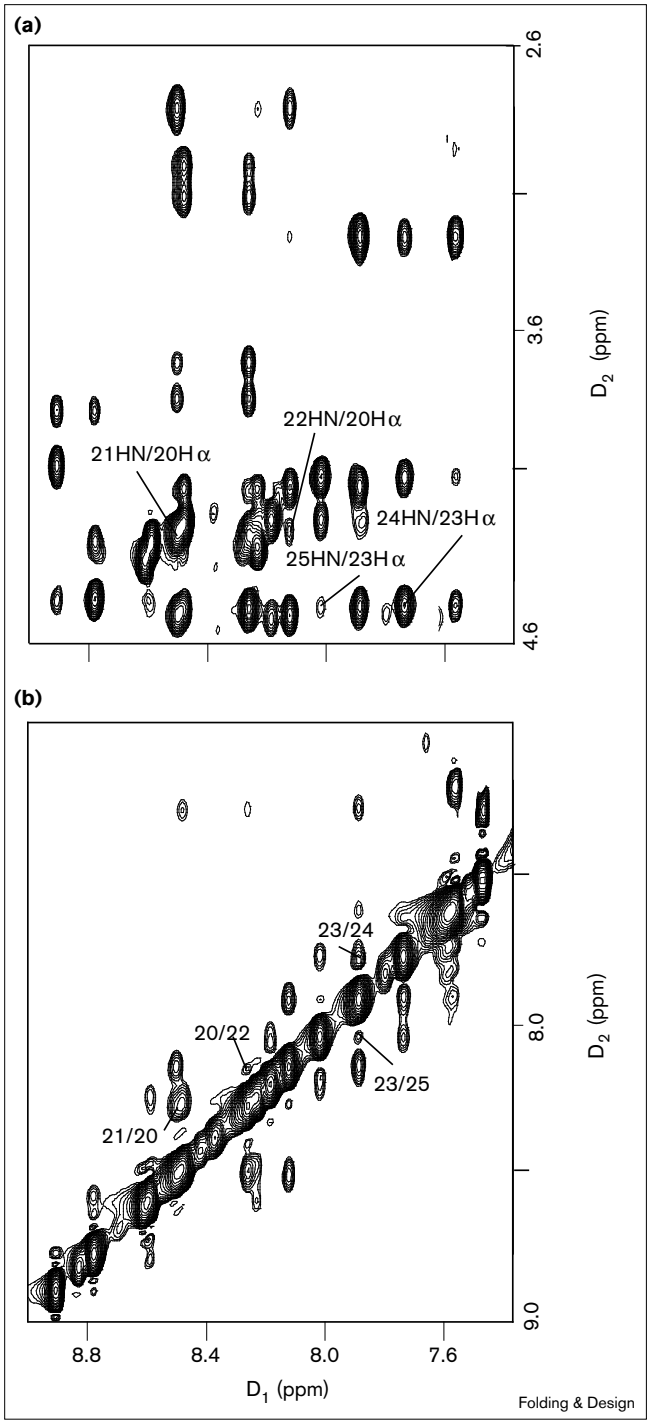

NOESY spectrum of wild-type p53 peptide showing the **(a)** $d_{\alpha N}$ and **(b)** d_{NN} regions. The characteristic NOEs for turn structures are indicated. The spectrum was acquired at 2°C with 10 mM wild-type p53 peptide in 90%H_2O/10%D_2O, 10 mM sodium phosphate, pH 6.0.

between 6 Hz and 8 Hz. These coupling constants do not agree with either type I or type II turns. Additional evidence for the conformational preference of the wild-type p53 peptide is provided by temperature coefficients. The temperature dependence of an amide proton chemical shift is an indication of protection from solvent, often by hydrogen bonds. Burial due to proximity of a bulky aromatic sidechain can also cause a small temperature coefficient [23]. For a random-coil peptide in water, the temperature coefficients of the amide protons are expected to be between 6 ppb/K and 10 ppb/K. For structured peptides having amide protons protected from the solvent, the temperature coefficients are generally below 6 ppb/K. Residues Leu22 to Leu25 have the lowest temperature coefficients among all residues in the peptide (Figure 4), suggesting that the amide protons of these residues may be better protected from the solvent than the other residues in the peptide. Other than Lys24, the temperature coefficients of residues Leu22–Leu25 are close to 6 ppb/K, also indicating significant conformational flexibility. Protection of the amide protons from the solvent suggested by temperature coefficients is consistent with amide proton chemical shift deviations from random-coil values.

Other strong evidence that the wild-type p53 peptide deviates significantly from a random-coil structure comes from many additional medium-range and long-range NOEs observed for this peptide, in addition to the medium-range NOEs described above (Figure 4). In particular, many NOEs have been observed among the backbone and sidechain protons of four hydrophobic and aromatic residues: Phe19, Leu22, Trp23 and Leu25 (Table 1). These NOEs would not be expected for a random-coil structure. A region of the 300 ms mixing time NOESY spectrum shown in Figure 6 demonstrates some of these NOEs. These observations indicate that a hydrophobic cluster tends to be formed by these residues. Interactions among these residues appear to be important for stabilizing the structural propensity of the wild-type p53 peptide. From a qualitative analysis of the NOEs involving the four hydrophobic and aromatic residues, however, it is not clear how these residues may interact with one another. In order to obtain a better understanding of the structural propensity of the p53 peptide and how the hydrophobic residues may interact with each other, structures of this peptide were calculated based on observed NOE and coupling constant data.

Structure calculation of the wild-type p53 peptide

Linear peptides are generally very flexible and exist as a conformational ensemble of a large number of widely different conformers in aqueous solution. Conformational parameters obtained from NOE and coupling constants are population-weighted average values. Therefore, complete characterization of all the conformations of a short linear peptide in aqueous solutions has been difficult and remains an area of active study. In many cases, one particular structure or family of structures cannot satisfy all NOE and coupling constant constraints, so calculations

Table 1

NOEs among Phe19, Leu22, Trp23 and Leu25 in wild-type p53 at pH 6.0, 2°C.

Phe19 αH	Leu22 $\delta CH_3(1)$
Phe19 αH	Leu22 $\delta CH_3(2)$
Phe19 αH	Leu25 $\delta CH_3(1)$
Phe19 αH	Leu25 $\delta CH_3(2)$
Phe19 β_2H	Leu22 β2H
Phe19 β_2H	Leu22 β_3H
Phe19 β_3H	Leu22 β_2H
Phe19 β_3H	Leu22 β_3H
Phe19 β_2H	Leu22 $\delta CH_3(1)$
Phe19 β_2H	Leu22 $\delta CH_3(2)$
Phe19 β_3H	Leu22 $\delta CH_3(1)$
Phe19 β_3H	Leu22 $\delta CH_3(2)$
Phe19 β_2H	Leu25 $\delta CH_3(1)$
Phe19 β_2H	Leu25 $\delta CH_3(2)$
Phe19 β_3H	Leu25 $\delta CH_3(1)$
Phe19 β_3H	Leu25 $\delta CH_3(2)$
Phe19 2,6H	Leu22 NH
Phe19 2,6H	Leu22 β_2H
Phe19 2,6H	Leu22 β_3H
Phe19 2,6H	Leu22 $\delta CH_3(1)$
Phe19 2,6H	Leu22 $\delta CH_3(2)$
Phe19 2,6H	Leu25 $\delta CH_3(1)$
Phe19 2,6H	Leu25 $\delta CH_3(2)$
Phe19 3,5H	Leu22 $\delta CH_3(1)$
Phe19 3,5H	Leu22 $\delta CH_3(2)$
Phe19 3,5H	Leu25 $\delta CH_3(1)$
Phe19 3,5H	Leu25 $\delta CH_3(2)$
Phe19 3,5H	Trp23 4H
Phe19 3,5H	Trp23 7H
Leu22 αH	Trp23 NH
Leu22 αH	Trp23 2H
Leu22 αH	Leu25 $\delta CH_3(1)$
Leu22 αH	Leu25 $\delta CH_3(2)$
Leu22 β_2H	Leu22 $\delta CH_3(1)$
Leu22 β_2H	Leu22 $\delta CH_3(2)$
Leu22 β_2H	Trp23 NH
Leu22 β_3H	Trp23 NH
Leu22 β_3H	Trp23 6H
Leu22 NH	Trp23 NH
Leu22 NH	Trp23 4H
Leu22 $\delta CH_3(1)$	Trp23 NH
Leu22 $\delta CH_3(2)$	Trp23 NH
Leu22 $\delta CH_3(1)$	Trp23 βH
Leu22 $\delta CH_3(2)$	Trp23 βH
Leu22 $\delta CH_3(1)$	Trp23 4H
Leu22 $\delta CH_3(2)$	Trp23 4H
Leu22 $\delta CH_3(1)$	Trp23 5H
Leu22 $\delta CH_3(2)$	Trp23 5H
Leu22 $\delta CH_3(1)$	Trp23 7H
Leu22 $\delta CH_3(2)$	Trp23 7H
Trp23 NH	Leu25 NH
Trp23 αH	Leu25 NH
Trp23 βH	Leu22 $\delta CH_3(1)$
Trp23 βH	Leu22 $\delta CH_3(2)$
Trp23 4H	Leu25 NH
Trp23 4H	Leu25 $\delta CH_3(1)$
Trp23 4H	Leu25 $\delta CH_3(2)$
Trp23 5H	Leu25 β2H
Trp23 5H	Leu25 β_3H
Trp23 5H	Leu25 $\delta CH_3(1)$
Trp23 5H	Leu25 $\delta CH_3(2)$
Trp23 6H	Leu25 $\delta CH_3(1)$
Trp23 6H	Leu25 $\delta CH_3(2)$
Trp23 7H	Leu25 $\delta CH_3(1)$
Trp23 7H	Leu25 $\delta CH_3(2)$

Figure 6

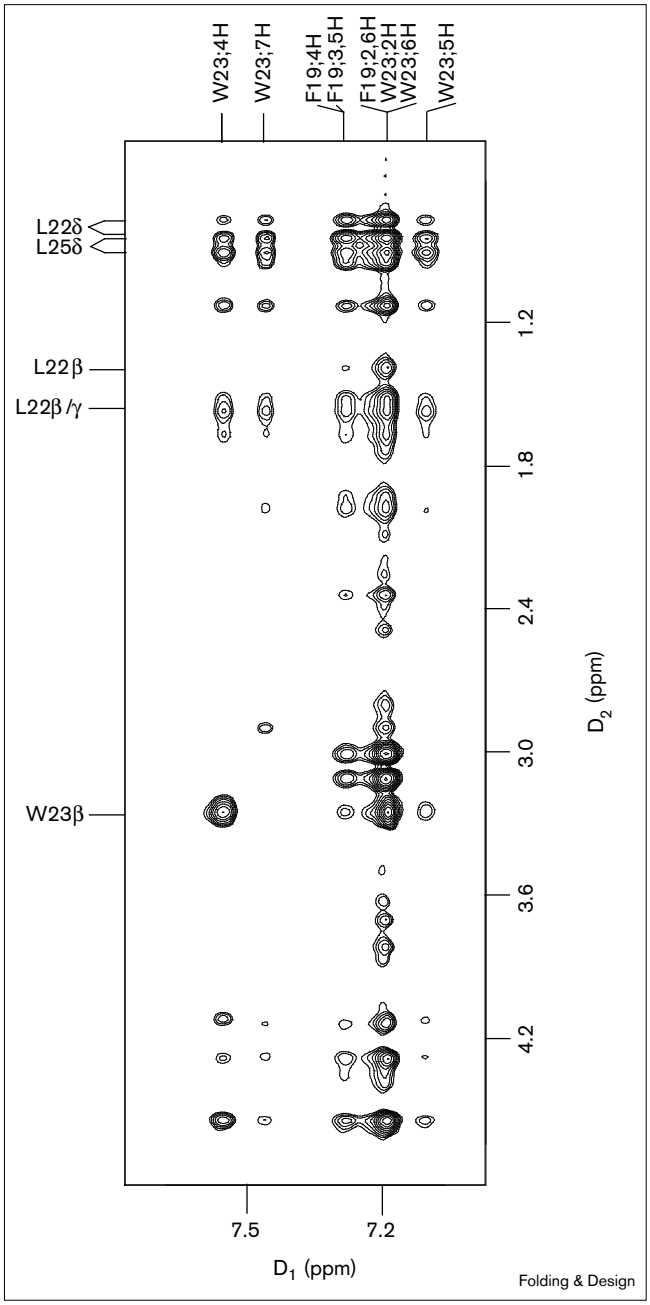

NOESY spectrum of the wild-type p53 peptide showing some NOEs among the hydrophobic and aromatic sidechains. The sample contained 10 mM p53 peptide dissolved in D_2O with 10 mM phosphate buffer, pH 6.0.

assuming multiple conformers need to be performed [38–40]. In the calculation with the wild-type p53 peptide, it was first assumed that all the nonsequential NOEs and nonrandom coil coupling constants result from one family of structures with a significant population. The resulting family of structures has favorable molecular mechanics

Table 2

NMR structure statistics.

(a) NMR constraints	
Distance constraints	234
Intraresidue	111
Sequential ($\|i-j\| = 1$)	73
Medium range ($1 < \|i-j\| \leq 4$)	40
Long range ($\|i-j\| > 4$)	10
Dihedral angle constraints	3
Φ	3
(b) Structure statistics	
NOE constraint violations per structure:	
Number > 0.1 Å	1.20 ± 1.01
Maximum violations (Å)	0.12 ± 0.03
Maximum dihedral angle violations	3.22 ± 1.39
AMBER energy (kcal/mol)	−130.54 ± 9.12
Van der Waals' energy (kcal/mol)	−55.46 ± 4.97
Angle energy (kcal/mol)	23.86 ± 1.87
Bond energy (kcal/mol)	2.93 ± 0.13
(c) RMS deviations from the mean structure	
Backbone heavy atoms (N, CA, C′, O)	
Residues 1–15	2.51
Residues 6–12	0.79
All heavy atoms	
Residues 1–15	3.02
Residues 6–12	0.91

energies and low constraint violations (Table 2). A few additional NOE constraints (approximately six) that were not used in the calculation were the weakest and had intensities close to the noise level. It is possible that these NOE constraints arose from minor conformations. The calculated structures are consistent with the covalent geometry and all experimental data, including coupling constants, that are not explicitly included in the calculation. Therefore, this family of structures may represent a significant population of structured conformers of the wild-type p53 peptide and provide further understanding of the mechanism of how the structure may be stabilized.

The backbone fold of the structures of the p53 peptide is shown in Figure 7. The 15 molecular dynamics refined structures from the 50 DIANA structures with the lowest constraint violations were used for detailed analysis. Statistics for the family of structures are summarized in Table 2. The conformation of the polypeptide backbone between residues Phe19 and Leu25 is well defined, whereas the residues close to both termini exhibit high disorder. The well-defined structure for the region Phe19–Leu25 is due to numerous nonsequential NOE constraints and dihedral angle constraints. In fact, all nonsequential NOE constraints observed are among the backbone and sidechain protons within residues Phe19–Leu25 (Figure 8).

The segment Phe19–Leu25 forms two turns as shown in the superposition of the backbone fold of the family of structures (Figure 7). The first turn runs from Phe19 to Leu22; the second turn commences at Leu22 and terminates at Leu25. The Φ and Ψ angles of the first turn exhibit considerable flexibility. For residues Ser20 and Asp21, the Φ angles range from –141° to 99° and from –115° to –56°, respectively. The measured $^3J_{HN\alpha}$ coupling constants for Ser20 and Asp21 are 7.3 Hz and 7.0 Hz, respectively, which are consistent with the Φ angles. Although it is not possible to assign the turn type of residues 19–22 based on the backbone dihedral angles of

Figure 7

Stereoview of the backbone conformation of 15 structures of the wild-type p53 peptide. The structures are superimposed to minimize the root mean square deviation of the backbone C′, Cα and N atoms of residues Phe19–Leu25.

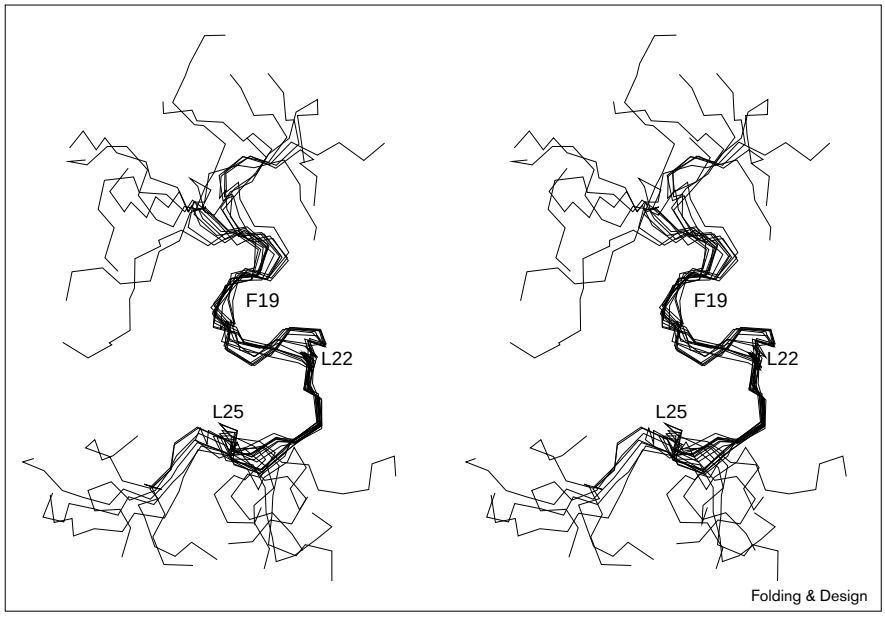

Figure 8

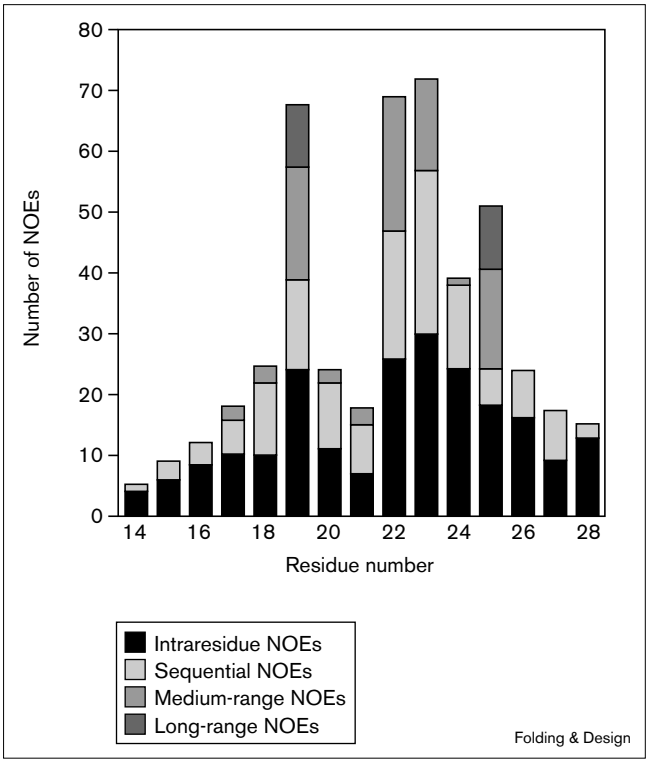

Plot of the number of NOE constraints versus residue number of the wild-type p53 peptide. Intraresidue NOEs, sequential NOEs, medium-range NOEs (between residues that are 2–4 residues apart in the primary sequence), and long-range NOEs (between residues that are five or more residues apart in the primary sequence) are indicated.

individual structures, the average Φ and Ψ angles of all structures (average Φ angles for residues 20 and 21 are –21° and –86°, and Ψ angles are –39° and –35°, respectively) agree best with a type III turn [41]. The backbone dihedral angles of Trp23 and Lys24 are better defined. The Φ angles of Trp23 and Lys24 range from –64° to –35° and from –74° to –55° and are both consistent with the measured $^3J_{HN\alpha}$ coupling constants of 5.5 Hz and 6.8 ± 1.2 Hz, respectively. The Φ dihedral angles of other residues are all consistent with the measured $^3J_{HN\alpha}$ coupling constants. In particular, residues at both C and N termini have $^3J_{HN\alpha}$ values reflective of the high conformational flexibility in these regions.

As indicated by NOE data, a hydrophobic cluster is formed by residues Phe19, Leu22, Trp23 and Leu25. The superposition of sidechain heavy atoms of residues 19–25 in the family of structures is shown in Figure 9a and a space-filling model of a representative structure is shown in Figure 9b. The sidechain of Leu22 packs on the aromatic rings of Phe19 and Trp23. The two aromatic residues also interact closely with each other. Residue Leu25 interacts with both aromatic rings and with Leu22. The hydrophobic interactions and aromatic ring stacking effect are responsible for stabilization of the structure of residues 19–25. The amide proton of Lys24 is partially buried in the hydrophobic cluster and protected from the solvent, consistent with its low temperature coefficient and upfield-shifted amide proton chemical shift. A secondary stabilization factor appears to be the charge interaction between Asp21 and Lys24. These two oppositely charged residues flank the hydrophobic cluster composed of residues Phe19, Leu22, Trp23 and Leu25. The sidechain of Lys24 is slightly ordered due to interactions with the hydrophobic cluster; the γH of Lys24 has NOEs with the ring protons 1H, 4H and 5H of Trp23. Close interaction of the Lys24 γH is also evident from the unusually upfield-shifted chemical shift (1.09 ppm).

Discussion

The double-turn structure

This study shows that the essential region of the p53 transactivation domain, residues 14–28, tends to form two β turns and is stabilized both by hydrophobic/aromatic and charged interactions. Interactions among amino acid sidechains have been found to play important roles in stabilizing structures in other short peptides or local structures in denatured proteins. These induce conformational preferences of amino acid residues to deviate from random-coil structures. In particular, hydrophobic and aromatic amino acid interactions appear to be important in stabilizing structures in aqueous solution. For example, urea-denatured 434 repressor contains a hydrophobic cluster that is formed by residues Val54, Val56, Trp58 and Leu59 [42]. The hydrophobic cluster results in the observation of a significant number of medium-range NOEs, which would not be expected for a random coil. Other examples of structures stabilized by hydrophobic and aromatic interactions include a 16-residue peptide forming a β hairpin [43] and a six-residue peptide forming a type VI turn [44]. Interactions involving charged sidechains can also play an important role in stabilizing secondary structures. This is shown in the S-peptide from ribonuclease A, where sidechain interactions between *i* to *i*+4 Phe and His, Glu and Lys, and Glu and Asp stabilized the helical structure in the peptide [45]. The structure of the wild-type p53 peptide provides further understanding of the mechanism by which conformational preferences of peptides are defined by the primary sequence.

The two β turns within the p53 transactivation domain appear to form cooperatively. This is demonstrated by the significant number of NOEs involving residues from both turns. Hydrophobic/aromatic interactions and charge interactions stabilizing the double-turn structure involve residues from both turns. A large number of NOEs were observed between the sidechains of Phe19 and Trp23 and between the sidechains of Phe19 and Leu25. Also, the sidechain protons of Leu22 have numerous NOEs to the

Figure 9

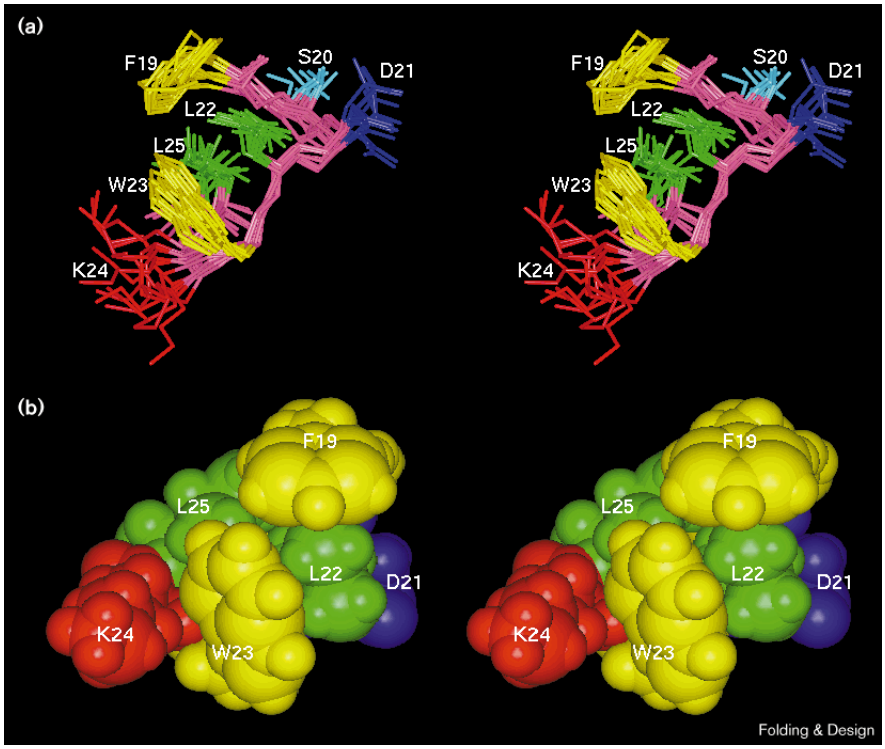

(a) Sidechain orientations from residues Phe19–Leu25 of 15 solution structures of the wild-type p53 peptide. The structures have been superimposed by the root mean square best fit of the backbone atoms of these residues. Backbone atoms are shown in pink, and sidechains are labeled. **(b)** Space-filling model showing the hydrophobic interaction of residues Phe19, Leu22, Trp23 and Leu25. The two charged residues, Asp21 and Lys24, are located on opposite sides of the hydrophobic cluster.

sidechain protons of Phe19, Trp23 and Leu25. The two residues, Asp21 and Lys24, that appear to be involved in electrostatic interaction also belong to two different turns. These data indicate that the two turns form cooperatively. To the best of our knowledge, this is the first short linear peptide in which a two-turn structure is preferred.

Structural propensity and bound conformations

Our studies indicate that the peptide segment Leu14–Glu28 of p53 has the propensity to form two reverse-turn structures with the functionally important residues Phe19, Leu22, Trp23 and Leu25 forming a hydrophobic cluster. Phe19, Leu22 and Trp23 maintain 100% identity among all the p53 sequences known to date, and Leu25 is conserved in p53 molecules from most species [46]. Substitutions Leu22→Gln and Trp23→Ser result in the loss of the structural propensity of the p53 peptide. The loss of the structural propensity is clearly due to the disruption of the hydrophobic cluster, but not the intrinsic preference of their backbone conformation. In a random peptide, the predicted distribution of Leu in α-helical conformation is 53% and in a β-strand conformation is 42% [37]. The intrinsic distribution of Gln in α-helical and β-strand conformations is 57% and 34%, respectively. Trp and Ser are equally populated between α-helical and β-strand conformations in a random-coil peptide. Thus, the amino acid substitutions do not change the intrinsic preferences for the backbone dihedral angles of the peptide. Instead, these substitutions perturb the hydrophobic interactions between the amino acid sidechains. Substitutions at residues 22 and 23 severely limit transcriptional activation and impair p53 binding to TFIID, mdm-2 and E1B 55K (Figure 10). From the structure of the p53–mdm-2 complex [26], Trp23 makes critical contacts with mdm-2. The substitutions not only disrupt the structural propensity of the wild-type p53 peptide, but would also be predicted to disrupt one of the important contacts with mdm-2.

On the basis of the structures of the free p53 peptide and the p53 peptide in complex with mdm-2, we propose a mechanism for the binding of p53 with mdm-2. In the crystal structure of a p53 peptide–mdm-2 complex, residues 18–26 of the p53 peptide form a helical structure [26]. In the solution structures of the free peptide, this same region favors two type III β turns with Φ and Ψ angles similar to those of helices. For example, the Φ angles of residues 19, 21, 22, 23 and 24 in the calculated structures are -68 ± 10^{o}, -86 ± 29^{o}, -64 ± 11^{o}, -50 ± 15^{o}, and -64 ± 10^{o}, respectively. The Ψ angles of residues 20 and 21 are -39 ± 29^{o} and -24 ± 10^{o}, respectively. These dihedral angles do not need to change significantly upon mdm-2 recognition. Three residues of the p53 transactivation domain, Phe19, Trp23 and Leu26, make critical contacts with mdm-2. Phe19 and Trp23 in the free peptide are in a poised position for recognition by mdm-2. Some residues within the double-turn region of the free p53 peptide

Figure 10

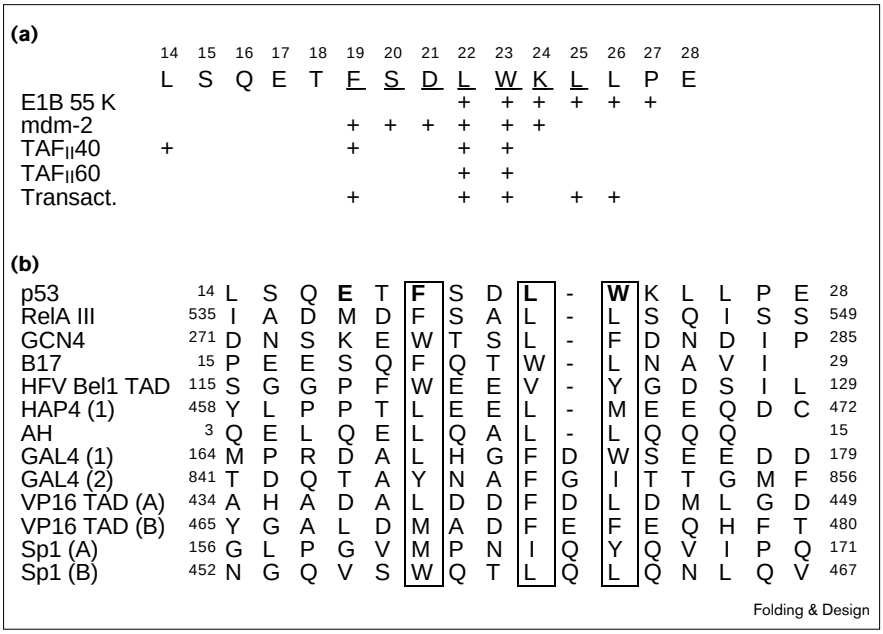

(a) Summary of mutagenesis data for p53 binding to several p53-binding proteins and for transactivation. Underlined residues are in the double-turn structure. 'Transact.' denotes transactivation activity. Plus signs denote residues that, when replaced singly or in combination with a second residue, inhibit binding to the indicated protein or prevent transactivation by at least 70%. Transactivation data are from [7,18], E1B 55K binding data from [18], mdm-2 binding data from [18,19,57], and $TAF_{II}40$ and $TAF_{II}60$ binding data from [9–11]. **(b)** Alignment of the p53 transactivation domain with other transactivation domains (based on the original data from [7,47]). Boldface residues in the p53 sequence share 100% identity across all species reported to date [46]. Boxed regions indicate conservation of bulky hydrophobic residue positions. Information on the transactivation domains is from the following sources: RelA III [58], GCN4 [59], B17 [60], human foamy virus (HFV) Bel1 transactivation domain (TAD) [61], HAP4 (1) [62], AH [50], GAL4 [63], VP16 TAD (A) [47], VP16 TAD (B) [64], Sp1 (A) and (B) [65].

appear to have high flexibility. For example, the Φ angles of residues 20 and 25 are -21 ± 120^{o} and -69 ± 59^{o}, respectively. The Ψ angles of residues 22, 24 and 25 are 143 ± 88^{o}, -16 ± 49^{o} and -13 ± 74^{o}, respectively. Upon mdm-2 binding, Leu22 interacts with mdm-2 without a significant change in its orientation and stabilizes the backbone dihedral angles around it into helical configurations. The binding of the third critical residue, Leu26, to mdm-2 stabilizes the dihedral angle around Leu25 and induces a change in the orientation of Leu25. Mutagenesis data have shown that mutation of Leu25 to Ala significantly reduces the affinity of p53 to mdm-2, although it does not form contacts with mdm-2 in the complex [19]. Based on the structural propensity of the free peptide, the sidechain of Leu25 helps to stabilize the hydrophobic cluster and may, thus, be required for proper presentation of the hydrophobic residues to mdm-2.

The structural propensity of the free peptide is reflected in the bound conformation when the peptide is in complex with mdm-2. In both the free and mdm-2-bound p53 peptide, the backbone conformations are similar. In addition, the sidechains of Phe19, Leu22 and Trp23 have similar relative orientations and maintain their contacts. In the NMR study of the bound conformation of a p53 peptide in complex with mdm-2, hydrophobic clustering of Phe19, Leu22, Trp23 and Pro24 (Lys24 was replaced by a Pro in this study) has also been observed as studied by transfer NOE methods [27]. The bound conformation of p53 when complexed with mdm-2 reflects the inherent structural propensity of the free p53 peptide, and this propensity may also be preserved when p53 is in complexes with $TAF_{II}40$, $TAF_{II}60$ and E1B 55K.

Structure and transactivation

The position pattern of Phe19, Leu22 and Trp23 is conserved among several transcription factors containing acidic, glutamine-rich or proline-rich domains [7,47]. An extensive alignment of such domains, shown to be critical for transactivation function, is presented in Figure 10b. One transactivator within this class that has been analyzed in some detail is VP16 expressed by herpes simplex virus type I [47]. The Leu22 counterpart of p53, Phe442 of the VP16 transactivation domain (A), could be replaced with Tyr but not Ser or Ala for effective transactivation. This suggests that a bulky hydrophobic residue at this position is critical for this function. The transactivation domain of VP16 can substitute for the N terminus of p53 to mediate transcriptional activation as well as downstream functions such as cell cycle arrest and apoptosis [48,49]. Another transactivation domain within this class is the AH peptide [50] (see Figure 10b). This 15 amino acid peptide can confer transactivation activity when fused onto the GAL4 DNA-binding domain. Further studies are needed to establish whether similar structural propensities exist within other proteins that regulate transcription through binding TFIID.

Materials and methods

Sample preparation

The 15 amino acid residue peptides LSQETFSDLWKLLPE (wild-type p53) and LSQETFSDQSKLLPE (mutant p53) were synthesized by solid phase method and purified by reverse phase HPLC. The amount of each peptide was calculated from the absorbance of Phe19 at

255 nm using the extinction coefficient value of 162 OD/mmol. Samples contained approximately 0.2–10 mM of the wild-type or the mutant p53 peptides, in either D_2O or 90%H_2O/10%D_2O of 10 mM sodium phosphate buffer, pH 6.0.

NMR measurements

NMR spectra were acquired on a Varian Unity-plus spectrometer operating at 500 MHz for protons. Internal 2,2-dimethyl-2-silapentane-5-sulfonic acid (DSS) was used as the proton chemical shift reference. Most experiments were carried out at 2°C. TOCSY [51] experiments were also done at 5, 10, 15 and 20°C for temperature coefficient measurements. A PE-COSY experiment [52] was performed on the wild-type peptide sample in D_2O. The $J_{\alpha\beta}$ coupling constants were measured for residues with nondegenerate βH resonances. Only residue Leu22 gave $J_{\alpha\beta}$ coupling constants of 4 Hz and 10 Hz corresponding to the two βH protons. Due to overlap of the γH resonance with one of the βH resonances of Leu22, however, further determination of the χ1 dihedral angle for Leu22 was not performed. Other residues gave coupling constants around 7 Hz, indicative of conformational averaging. NOESY, TOCSY and DQF-COSY experiments were performed on both D_2O and 90%H_2O/10%D_2O solubilized samples of the wild-type and mutant peptides. The NOESY spectra were collected using 50–500 ms mixing times. The TOCSY spectra were acquired using isotropic mixing times of 30 ms and 70 ms. All spectra were processed using Felix 95 software (Molecular Simulations, Inc.).

The diffusion coefficients of the peptides were measured using the pulsed-field gradient method [30]. Ten gradient strengths, 3.68, 5.52, 7.36, 9.92, 11.0, 12.9, 14.7, 16.6, 18.4 and 20.2 Guass/cm, were used in the measurements. In the gradient experiments, Shigemi NMR tubes (Shigemi, Inc., Japan) were used, wherein 1 cm length samples were centered along the radio frequency coil (1.5 cm long). This warrants that the sample is in the linear region of the gradient strength. The ln(echo amplitudes), ln(A), were plotted versus the square of the gradient strengths, g^2. The slope of these plots can be used to calculate diffusion coefficients (D_s) as given by equation 1:

$$\ln(A) = \ln(A_o) - (\gamma\delta g)^2\left(\left(\Delta - \frac{\delta}{3}\right)D_s\right) \quad (1)$$

Generation of constraints

Distance information was obtained from NOESY spectra at 300 ms mixing time, on both D_2O and 90%H_2O/10%D_2O samples of the wild-type peptide. Distance constraints were determined from cross-peak volumes by calibration against known distances. Upper bounds were assigned as 3.0, 3.7, 4.0, 5.0 and 6.0 Å. On these upper bounds, pseudoatom corrections were incorporated in the calculation of initial structures with the program DIANA [53]. In the refinement of these initial structures with the program AMBER [54], distance corrections were achieved by r^{-6} averaging. Lower bounds were the van der Waals' radii. Dihedral angle constraints were obtained from coupling constant measurements. From the DQF-COSY spectrum, $^3J_{HN\alpha}$ were determined for 13 residues ([55]; Figure 4). Residues having $^3J_{HN\alpha} < 6$ Hz have their Φ angles constrained to −90° to 40° in the DIANA calculations, and −90° to −40° in the AMBER calculations. In the AMBER calculations, the ω angles of the peptide backbone were constrained in all cases to be 180° ± 5°. The peptide bond preceding Pro27 is mainly in the *trans* conformation.

Structure calculations

Initial peptide structures were calculated with the program DIANA [53] using the redundant dihedral angle constraint (REDAC) strategy [56]. To the 50 initial randomized structures, three cycles of REDAC were applied followed by a single cycle using only experimental constraints.

All 50 structures generated by DIANA had target functions from 0.19 to 1.13 and were then refined using a combination of energy minimization and restrained molecular dynamics with the AMBER program. In these calculations, the charge of residues Lys, Asp and Glu were reduced by 80% and a distance-dependent dielectric constant was used to account for calculation in vacuum. The first energy minimization consisted of 200 steps after which the target temperature was increased to 1200K for 4 ps. The structures were then annealed for 10 ps with a target temperature of 0K, followed by a 1 ps energy 'quench'. The final phase of the refinement consisted of 200 steps of conjugate gradient energy minimization. During the initial energy minimization and the first 3 ps of molecular dynamics, the force constant for the distance constraint violations was increased from 0 to 32 kcal/(Å^2 mol) and maintained at this value throughout the annealing and final minimization steps. The force constant for dihedral angle constraint violations was also increased in a similar manner as above from 0 to 20 kcal/mol for Φ. For the chirality and ω angle constraints, the force constants were set to 50 and 20 kcal/mol, respectively.

Supplementary material

Chemical shift assignments and NOE buildup curves of a few typical crosspeaks are provided as supplementary material.

Acknowledgements

We thank Garry Gippert for providing us the programs ROTFIX and ICOMPARE for the analyses of our structures. We appreciate helpful comments on the manuscript from Wayne J Fairbrother, Maria Mas and Gerard Zambetti. This work is supported by NIH GM 54190 and American Cancer Society Junior Faculty Research Award JFRA-646 to Y.C., and UCBCRP 1KB-0102 to J.M.

References

1. Maltzman, W. & Czyzyk, L. (1984). UV irradiation stimulates levels of p53 cellular tumor antigen in nontransformed mouse cells. *Mol. Cell. Biol* **4**, 1689-1694.
2. Kastan, M.B., Onyekwere, O., Sidransky, D., Vogelstein, B. & Craig, R.W. (1991). Participation of p53 protein in the cellular response to DNA damage. *Cancer Res.* **51**, 6304-6311.
3. Gottlieb, T.M. & Oren, M. (1996). P53 in growth control and neoplasia. *Biochim. Biophys. Acta* **1287**, 77-102.
4. Ko, L.J. & Prives, C. (1996). P53: puzzle and paradigm. *Genes Dev.* **10**, 1054-1072.
5. Fields, S. & Jang, S. (1990). Presence of a potent transcription activating sequence in the p53 protein. *Science* **249**, 1046-1049.
6. Raycroft, L., Wu, H. & Lozano, G. (1990). Transcriptional activation by wild-type but not transforming mutants of p53 anti-oncogene. *Science* **249**, 1049-1051.
7. Chang, J., Kim, D.H., Lee, S.W., Choi, K.Y. & Sung, Y.C. (1995). Transactivation ability of p53 transcriptional activation domain is directly related to the binding affinity to TATA-binding protein. *J. Biol. Chem.* **270**, 25014-25019.
8. Seto, E., *et al.*, & Shenk, T. (1992). Wild-type p53 binds to the TATA-binding protein and represses transcription. *Proc. Natl Acad. Sci. USA* **89**, 12028-12032.
9. Lu, H. & Levine, A.J. (1995). Human $TAF_{II}31$ protein is a transcriptional coactivator of the p53 protein. *Proc. Natl Acad. Sci. USA* **92**, 5154-5158.
10. Thut, C.J., Chen, J.-L., Klemm, R. & Tijian, R. (1995). P53 transcriptional activation mediated by coactivators $TAF_{II}40$ and $TAF_{II}60$. *Science* **267**, 100-103.
11. Farmer, G., Colgan, J., Nakatani, Y., Manley, J.L. & Prives, C. (1996). Functional interaction between p53, the TATA-binding protein (TBP), and TBP-associated factors *in vivo. Mol. Cell. Biol.* **16**, 4295-4304.
12. Oliner, J.D., Kinzler, K.W., Meltzer, P.S., George, D.L. & Vogelstein, B. (1992). Amplification of a gene encoding a p53-associated protein in human sarcomas. *Nature* **358**, 80-83.
13. Momand, J. & Zambetti, G.P. (1997). Mdm-2: 'big brother' of p53. *J. Cell. Biochem.* **64**, 343-352.
14. Momand, J., Zambetti, G.P., Olson, D.C., George, D. & Levine, A.J. (1992). The mdm-2 oncogene product forms a complex with the p53 protein and inhibits p53-mediated transactivation. *Cell* **69**, 1237-1245.
15. Yew, P.R. & Berk, A.J. (1992). Inhibition of p53 transactivation required for transformation by adenovirus early 1B protein. *Nature* **357**, 82-85.
16. Oliner, J.D., Pietenpol, J.A., Thiagalingam, S., Gyuris, J., Kinzler, K.W. & Vogelstein, B. (1993). Oncoprotein MDM2 conceals the activation domain of tumor suppressor p53. *Nature* **362**, 857-860.

17. Chen, J., Marechal, V. & Levine, A.J. (1993). Mapping of the p53 and mdm-2 interaction domains. *Mol. Cell. Biol.* **13**, 4107-4114.
18. Lin, J., Chen, J., Elenbaas, B. & Levine, A.J. (1994). Several hydrophobic amino acids in the p53 amino-terminal domain are required for transcriptional activation, binding to mdm-2 and the adenovirus 5 E1B 55-kD protein. *Genes Dev.* **8**, 1235-1246.
19. Picksley, S.M., Vojtesek, B., Sparks, A. & Lane D.P. (1994). Immunochemical analysis of the interaction of p53 with MDM2: fine mapping of the MDM2 binding site on p53 using synthetic peptides. *Oncogene* **9**, 2523-2529.
20. Pavletich, N.P., Chambers, K.A. & Pabo, C.O. (1993). The DNA-binding domain of p53 contains the four conserved regions and the major mutation hot spots. *Genes Dev.* **7**, 2556-2564.
21. Dyson, H.J. & Wright, P.E. (1995). Antigenic peptides. *FASEB J.* **9**, 36-49.
22. Dyson, H.J., Rance, M., Houghten, R.A., Wright, P.E. & Lerner, R.A. (1988). Folding of immunogenic peptide fragments of proteins in water solution. II. The nascent helix. *J. Mol. Biol.* **201**, 201-217.
23. Kemmink, J. & Creighton, T.E. (1993). Local conformations of peptides representing the entire sequence of bovine pancreatic trypsin inhibitor and their roles in folding. *J. Mol. Biol.* **234**, 861-878.
24. Dyson, H.J. & Wright, P.E. (1993). Peptide conformation and protein folding. *Curr. Opin. Struct. Biol.* **3**, 60-65.
25. Itzhaki, L.S., Neira, J.L., Ruiz-Sanz, J., De Prat Gay, G. & Fersht A.R. (1995). Search for nucleation sites in smaller fragments of chymotrypsin inhibitor 2. *J. Mol. Biol.* **254**, 289-304.
26. Kussie, P.H., *et al*., & Pavletich, N.P. (1996). Structure of the MDM2 oncoprotein bound to the p53 tumor suppressor transactivation domain. *Science* **274**, 948-953.
27. Blommers, M.J.J., Fendrich, G., Garciaecheverria, C. & Chene, P. (1997). On the interaction between p53 and MDM2: transfer NOE study of a p53-derived peptide ligated to MDM2. *J. Am. Chem. Soc.* **119**, 3425-3426.
28. Marqusee, S., Robbins, V.H. & Baldwin, R.L. (1989). Unusually stable helix formation in short alanine-based peptides. *Proc. Natl Acad. Sci. USA* **86**, 5286-5290.
29. Lumb, K.J. & Kim, P.S. (1994). Formation of a hydrophobic cluster in denatured bovine pancreatic trypsin inhibitor. *J. Mol. Biol* **236**, 412-420.
30. Alteri, A.S., Hinton, D.P. & Byrd, R.A. (1995). Association of biomolecular systems via pulsed field gradient NMR self-diffusion measurements. *J. Am. Chem. Soc.* **117**, 7566-7567.
31. Holladay, L.A., Rivier, J. & Puett, D. (1977). Conformational studies on somatostatin and analogues. *Biochemistry* **16**, 4895-4900.
32. Wüthrich, K. (1986). *NMR of Proteins and Nucleic Acids*. Wiley-Interscience Publication, New York.
33. Wishart, D.S. & Sykes, B.D. (1994). Chemical shift as a tool for structure determination. *Methods Enzymol.* **239**, 363-439.
34. Wishart, D.S., Bigam, C.G., Holm, A., Hodges, R.S. & Sykes, B.D. (1995). ^{1}H, ^{13}C, ^{15}N random coil NMR chemical shifts of the common amino acids. I. Investigation of nearest neighbor effects. *J. Biomol. NMR* **5**, 67-81.
35. Fiebig, K.M., Schwalbe, H., Buck, M., Smith, L.J. & Dobson, C.M. (1996). Towards a description of the conformation of denatured states of proteins. Comparison of a random coil model with NMR measurements. *J. Phys. Chem.* **100**, 2661-2666.
36. Arcus, V.L., Vuilleumier, S., Freund, S.M.V., Bycroft, M. & Fersht, A.R. (1995). A comparison of the pH, urea and temperature-denatured states of barnase by heteronuclear NMR: implications for the initiation of protein folding. *J. Mol. Biol.* **254**, 305-321.
37. Smith, L.J., Bolin, K.A., Schwalbe, H., Macarthur, M.W., Thorton, J.M. & Dobson, C.M. (1996). Analysis of main chain torsion angles in proteins. Prediction of NMR coupling constants for native and denatured conformations. *J. Mol. Biol* **255**, 494-506.
38. Blackledge, M.J., Bruschweiler, R., Griesinger, C., Schmidt, J.M., Xu, P. & Ernst, R.R. (1993). Conformational backbone dynamics of the cyclic decapeptide antamanide. Application of a new multiconformational search algorithm based on NMR data. *Biochemistry* **32**, 10960-10974.
39. Nanzer, A.P., Poulson, F.M., van Gunsteren, W.F. & Torda, E.A. (1994). Reassessment of the structure of chymotrypsin inhibitor 2 (CT-2) using time-averaged NMR restraints. *Biochemistry* **33**, 14503-14511.
40. Bonvin, A.M.J.J., Boelens, R. & Kaptein, R.J. (1994). Time- and ensemble-averaged direct NOE restraints. *J. Biomol. NMR* **4**, 143-149.
41. Wilmot, C.M. & Thornton, J.M. (1988). Analysis and prediction of the different types of beta-turns in proteins. *J. Mol. Biol.* **203**, 221-232.
42. Neri, D., Billeter, M., Wider, G. & Wüthrich, K. (1992). Determination of the nuclear magnetic resonance solution structure of the DNA-binding domain (residues 1 to 69) of the 434 repressor and comparison with the X-ray crystal structure. *Science* **257**, 1559-1563.
43. Blanco, F.J., Rivas, G. & Serrano, L. (1994). A short linear peptide that folds into a native β-hairpin in aqueous solution. *Nat. Struct. Biol.* **1**, 584-590.
44. Yao, J., Dyson, H.J. & Wright, P.E. (1994). Three-dimensional structure of a type VI turn in a linear peptide in water solution. Evidence for stacking of aromatic rings as a major stabilizing factor. *J. Mol. Biol.* **243**, 754-766.
45. Baldwin, R.L. (1995). α-Helical formation by peptides of defined sequence. *Biophys. Chem.* **55**, 127-135.
46. Soussi, T. & May, P. (1996). Structural aspects of the p53 protein in relation to gene evolution: a second look. *J. Mol. Biol.* **260**, 623-637.
47. Cress, W.D. & Triezenberg, S.J. (1991). Critical structural elements of the VP16 transcriptional activation domain. *Science* **251**, 87-90.
48. Pietenpol, J.A. & Tokino, T. (1994). Sequence-specific transcriptional activation is essential for growth suppression by p53. *Proc. Natl Acad. Sci. USA* **91**, 1998-2002.
49. Attardi, L.D., Lowe, S.W., Brugarolas, J. & Jacks, T. (1996). Transcriptional activation by p53, but not induction of the p21 gene, is essential for oncogene-mediated apoptosis. *EMBO J.* **15**, 3693-3701.
50. Giniger, E. & Ptashne, M. (1987). Transcription in yeast activated by a putative amphipathic α-helix linked to a DNA-binding unit. *Nature* **330**, 670-672.
51. Cavanagh, J. & Rance, M. (1992). Suppression of cross relaxation effects in TOCSY spectra via a modified DIPSI-2. *J. Magn. Reson.* **96**, 670-678.
52. Mueller, L. (1987). PE-COSY, a simple alternative to E-COSY. *J. Magn. Reson.* **72**, 191-196.
53. Güntert, P., Braun, W. & Wüthrich, K. (1991). Efficient computation of three-dimensional protein structures in solution from nuclear magnetic resonance data using the program DIANA and the supporting programs CALIBA, HABAS and GLOMSA. *J. Mol. Biol.* **217**, 517-531.
54. Pearlman, D.A., *et al*., & Kollman, P.A. (1995). *AMBER 4.1*. University of California, San Francisco, USA.
55. Kim, Y. & Prestegard, J.H. (1989). Measurement of vicinal coupling from crosspeaks in COSY spectra. *J. Magn. Reson.* **84**, 9-13.
56. Güntert, P. & Wüthrich, K. (1991). Improved efficiency of protein structure calculations from NMR data using the program DIANA with redundant dihedral angle constraints *J. Biomol. NMR* **1**, 447-456.
57. Marston, N.J., Crook, T. & Vousden, K.H. (1994). Interaction of p53 with MDM2 is independent of E6 and does not mediate wild-type transformation suppressor function. *Oncogene* **9**, 2707-2716.
58. Blair, W.S., Bogard, H.P., Madore, S.J. & Cullen, B.R. (1994). Mutational analysis of the transcription activation domain of RelA: identification of a highly synergistic minimal acidic activation module. *Mol. Cell. Biol.* **14**, 7226-7234.
59. Hope, I.A., Mahadevan, S. & Struhl, K. (1988). Structural and functional characterization of the short acidic transcriptional activation region of yeast GCN4 protein. *Nature* **333**, 635-640.
60. Ma, J. & Ptashne, M. (1987). A new class of yeast transcriptional activators. *Cell* **51**, 113-119.
61. Lee, C.W., Chang, J., Lee, K.J. & Sung, Y.C. (1994). The Bel1 protein of human foamy virus contains one positive and two negative control regions which regulate a distinct activation domain of 30 amino acids. *J. Virol.* **68**, 2708-2719.
62. Forsburg, S.L. & Guarente, L. (1989). Identification and characterization of HAP4: a third component of the CCAAT-bound HAP2/HAP3 heteromer. *Genes Dev.* **3**, 1166-1178.
63. Wu, Y., Reece, R.J. & Ptashne, M. (1996). Quantitation of putative activator-target affinities predicts transcriptional activating potentials. *EMBO J.* **15**, 3951-3963.
64. Triezenberg, S.J., Kingsbury, R.C. & McKnight, S.L. (1988). Functional dissection of VP16, the trans-activator of herpes simplex virus immediate early gene expression. *Genes Dev.* **2**, 718-729.
65. Courey, A.J. & Tjian, R. (1988). Analysis of Sp1 *in vivo* reveals multiple transcriptional domains, including a novel glutamine-rich activation motif. *Cell* **55**, 887-898.

Because *Folding & Design* operates a 'Continuous Publication System' for Research Papers, this paper has been published via the internet before being printed. The paper can be accessed from http://biomednet.com/cbiology/fad.htm – for further information, see the explanation on the contents pages.